THE ASTROPHYSICAL JOURNAL, 407:100–109, 1993 April 10

THE IMPACT OF SUPERNOVA FRAGMENTS ON THE EVOLUTION OF MULTISUPERNOVA REMNANTS

J. FRANCO,[1] A. FERRARA,[2] M. RÓŻYCZKA,[3] G. TENORIO-TAGLE,[4] AND D. P. COX[5]
Received 1991 November 6; accepted 1992 September 25

ABSTRACT

The interaction of supernova fragments with the internal structure of large multisupernova remnants (MSRs) is studied with analytical approximations and two-dimensional hydrodynamical simulations. The fragments are thermalized by reverse shocks generated in the interaction with the MSR interior, which is assumed to be hot ($T \sim 10^7$ K) and rarefied (with a gas density $n \sim 10^{-2}$ to 10^{-3} cm^{-3}). The density and velocity stratifications of the supernova ejecta, which define the fragment properties, are taken from recent explosion models for Type II supernova. The evolution can be divided in two stages: before and after reaching a reference distance, R_E (where the fragment has been eroded by 5%), from the explosion site. At early times, when located interior to R_E, the fragment expands almost freely because the reverse shock is not able to penetrate to a significant depth (the reverse shock speed remains low because the fragment density is substantially higher than the MSR interior density). As the density of the expanding fragment drops, the reverse shock accelerates, and, when the distance R_E is reached, it begins to effectively erode the fragment. The erosion process is followed with both analytical approximations and numerical simulations, and we find a very good agreement between the two methods. At some selected evolutionary times, the X-ray emission from the shocked fragment is also calculated. When sequential SN explosions are considered, the key issue in the evolution of a multisupernova remnant is whether or not the fragments can survive until they collide with the MSR shell. This "bombardment" phase can last for about a few million years (or, at typical SN explosion rates on OB associations, up to the first approximated five to 10 explosions). This direct bombardment of the MSR shell has a series of important consequences: it excites, punctures, and deforms the expanding shell.

Subject headings: galaxies: ISM — hydrodynamics — ISM: bubbles — shock waves — supernova remnants

1. INTRODUCTION

The population of young massive stars represents a rich energy source for the interstellar gas, and the importance of this energy injection in structuring the general interstellar medium was pointed out since the mid-1970s (e.g., Cox & Smith 1974; Salpeter 1976; McKee & Ostriker 1977; Weaver et al. 1977). The idea that large-scale gaseous features could also be formed due to the collective action of stellar groups followed immediately (e.g., Reynolds & Ogden 1978, 1979; Cowie, Songaila, & York 1979; Heiles 1979; McCray & Snow 1979), and many observed structures in the Milky Way and other external galaxies have been ascribed to this stellar input (see review by Tenorio-Tagle & Bodenheimer 1988). In particular, the energy and momentum injection from OB associations may be responsible for many of the large-scale "holes" and "supershells" (or "superbubbles") observed in the Milky Way (e.g., Heiles 1979, 1984), M31 (e.g., Brinks & Bajaja 1986), and M33 (e.g., Deul & Hartog 1990). These large gaseous structures, with sizes in the range of about 10^2–10^3 pc, have swept-up masses in excess of 10^4 $M_\odot$ and kinetic energies ranging from about 10^{51} to several times 10^{53} ergs. Except for the largest and more energetic supershells, which can be better ascribed to the action of infalling high-velocity clouds (e.g., Tenorio-Tagle 1981; Tenorio-Tagle et al. 1987b; Franco et al. 1988; van der Hulst & Sancisi 1988; Alfaro, Cabrera-Caño, & Delgado 1991), most of these types of structures can be generated by expanding "multisupernova remnants" (MSRs) driven by typical young stellar groups.

The evolution of MSRs, which has been explored only during the last decade (e.g., Bruhweiler et al. 1980; Tomisaka Habe, & Ikeuchi 1981; Tomisaka & Ikeuchi 1986; McCray & Kafatos 1987; Tenorio-Tagle, Bodenheimer, & Różyczka 1987a; Mac Low & McCray 1988; Mac Low, McCay & Norman 1989; Igumentshchev, Shustov, & Tutukov 1990; Palouš, Franco, & Tenorio-Tagle 1990; Tenorio-Tagle et al. 1990a; Ferriére, Mac Low, & Zweibel 1991; Tomisaka 1992), leads to the formation of a rich variety of gaseous structures. Existing numerical models indicate that MSRs can produce cavities and shells with dimensions corresponding to the observed ones (see reviews by McCray 1988, Różyczka 1989, and Franco et al. 1992). These models already include the disk density stratification and, in a few cases, an external magnetic field or the shear due to the galactic differential rotation. Some of the resulting gas structures are associated with either Rayleigh-Taylor or flow instabilities in cooling shocks (e.g., Vishniac 1983; Tenorio-Tagle et al. 1987a; Kimura & Tosa 1988), whereas some other features are due to environmental

[1] Instituto de Astronomía–UNAM, Apdo. Postal 70-264, 04510 México D. F., México. e-mail (Internet): jjfranco@alfa.astroscu.unam.mx.
[2] Osservatorio Astrofisico de Arcetri, Italy. Postal address: Space Telescope Science Institute, 4700 San Martin Drive, Baltimore, MD 21218. e-mail (Bitnet): ferrara@astrfi.astro.it.
[3] University of Warsaw Observatory, Al. Ujazdowskie 4, PL-00478 Warszawa, Poland. Also Instituto di Astrofisica de Canarias, Spain. e-mail (Bitnet: mnr@plwauw61.
[4] Instituto de Astrofísica de Canarias, 38200 La Laguna, Tenerife, Spain. e-mail (Bitnet): gtt@iac.es.
[5] Department of Physics, University of Wisconsin–Madison, 1150 University Avenue, Madison, WI 53706. e-mail (Internet): cox% wisp.decnet@vms.macc.wisc.edu.

effects (i.e., accelerations due to the disk density gradient or to deformations and flows generated by galactic differential rotation).

Aside from these environmental effects, the details of shell evolution (along with the resulting gas structures) also depend on the way the matter and energy are injected into the expanding remnant. The injection from repeated supernova explosions has been simulated in numerical models as a pulsed mass and energy input but, in addition, there exists the possibility of having dense clumps (or fragments) in the supernova ejecta. Observational evidence for clumpy ejecta is growing and has been found in Cas A (see Braun, Gull, & Perley 1987 and references therein), SN 1987A (see Arnett, Fryxell, & Miller 1989 and Lucy et al. 1989), Tycho (e.g., Seward, Gorenstein, & Tucker 1983; Hamilton 1985), Puppis A (e.g., Winkler et al. 1988), Kepler (e.g., Bandiera & van den Bergh 1991), and a number of extragalactic remnants (e.g., Hamilton 1985; Lasker & Golinowski 1991). These examples already indicate that ejecta fragmentation could be a common process, and Rayleigh-Taylor instabilities seem to be its likely origin (Falk & Arnett 1973). The effects produced by the resulting fragments have been explored for the case of single SN explosions evolving in either a power-law ambient medium (Hamilton 1985) or inside a preexisting wind-driven shell (Tenorio-Tagle et al. 1991; see review by Franco et al 1991), or for SN fragments interacting with ambient clouds (McKee 1983). These effects, of course, depend on the clump properties and ambient conditions.

High-density fragments move almost unimpeded inside the wind-driven cavity, but they are rapidly thermalized at impact with the external shell. The fragment-shell interaction drives strong shocks at the places of impact which, aside from generating a variety of time-dependent features, can puncture and distort the original shell. The general properties of a wind-driven bubble are not very different from those of a MSR (i.e., a hot and low-density interior, surrounded by a cold and massive shell), and a logical step forward is to explore the effects of clumpy ejecta in the evolution of MSRs. Here we address this important topic and derive the evolution of a SN fragment inside a hot cavity with both an analytical approach and two-dimensional numerical simulations. The analytical formulation provides an adequate physical insight about the fragment-environment interactions and represents a useful (and much needed) tool to bypass the problems arising in numerical simulations when one has to follow the evolution over several orders of magnitude in scale (i.e., from the initial fragment size to the dimensions of MSRs). The two-dimensional hydrodynamical simulations, on the other hand, provide a more complete view of the interactions and a detailed evolution of the resulting transient features.

The paper is organized as follows. Section 2 discusses the most relevant processes governing fragment evolution and describes the penetration of the reverse shock along the fragment symmetry axis. The conditions for direct fragment-shell collision are also derived, and the evolution of the resulting X-ray spectrum, in the range 0.2–10 keV, is obtained. These approximated solutions are compared with the results of the detailed two-dimensional hydrodynamical simulations described in § 3, and a brief discussion is presented in § 4.

2. ANALYTICAL FORMULATION

The details of the interaction of an expanding fragment with its surrounding medium depend on the fragment properties. These, in turn, depend on the properties of the model ejecta, which define the structure of both the fragment and inter-fragment medium. Here we use the ejecta model for SN 1987A derived by Arnett (1988; see also Woosley et al 1988) and assume that it represents the interfragment medium of a typical supernova exploding inside a multi-SN shell. The radial density distribution of the ejecta becomes relaxed several hours after explosion and can be fitted by two power laws. The outmost parts, the atmosphere of the progenitor, contain a very small fraction of the ejected mass and are characterized by a steep density stratification with $\rho(r) \sim r^{-9}$. The rest of the ejecta, however, have a much shallower distribution with a dependence $\sim r^{-3}$. Thus, most of the ejected mass is in the r^{-3} stratification, and the fragment density distribution is assumed to follow this same power-law value. For convenience, the initial model is taken at $t_0 = 1.85$ days after explosion (see Fig. 4 of Arnett 1988). At this time, most of the ejecta lie between 10^{13} cm $< R_{ej} < 10^{14}$ cm, and the corresponding velocities are almost linearly stratified in radius within about 10^3 and 10^4 km s^{-1}.

2.1. *Fragmented Ejecta*

Numerical simulations indicate that the ejecta can become Rayleigh-Taylor–unstable shortly after the explosion, and that these instabilities can develop in either Type I or Type II supernovae (e.g., Chevalier & Klein 1978; Arnett et al. 1989; Fryxell, Arnett, & Müller 1991; Müller, Fryxell, & Arnett 1991; Nomoto et al. 1991; Hachisu et al. 1990, 1991). The model results, then, cover a wide range of progenitor masses, and the fragment densities are a factor of about 3–10 higher than the surrounding plasma. These values are probably limited by code resolution and one could expect larger fragment densities as a finer spatial resolution is achieved. Thus, here it is assumed that the density contrast between the fragment and interfragment medium, ϵ, is in the range of about 3–100.

The fragment density and velocity distributions are defined by their initial extents and locations. For Type I supernovae, with low-mass progenitors, the instabilities are initiated at the He/C + O interface, whereas for Type II SNs, they are initiated at the H/He boundary (e.g., Hachisu et al. 1990, 1991). For consistency with our chosen ejecta model, then, the initial fragment locations and radial extents are taken from the models of Arnett et al. (1989; see also Fryxell et al. 1991), which have addressed the particular fragmentation process of SN 1987A. These models follow the fragment evolution during a very short period of time but, in the absence of interactions (i.e., during the free expansion phase), the fragmented ejecta simply follow a homologous growth until they are processed by a reverse shock. The density contrast, ϵ, and the ratio between the fragment size and the radius of the ejecta, $l_0/R_{ej,0}$ (where l_0 is the initial fragment size and $R_{ej,0}$ is the initial radius of the ejecta), remain constant during the free expansion stage. A rough estimate (see Fig. 1 of Arnett et al. 1989) indicates that $l_0/R_{ej,0}$ is in the range of about 1/5 to 1/10, and these will be used as representative values of the clump sizes.

As discussed before, the initial inter-fragment density distribution is defined by Arnett's (1988) model at $t_0 = 1.85$ days after explosion. The initial radius of the ejecta is $R_{ej,0} = 10^{14}$ cm and the density distribution, which is truncated below 10^{13} cm, becomes

$$\rho_{ej}(t = t_0) = AR_{ej}^{-3}\,, \tag{2.1}$$

where $A = 10^{33}$ g (in cgs units), and R_{ej} is the location from the explosion center. The outermost layer of the ejecta has an initial density $AR_{ej,0}^{-3} = 10^{-9}$ g cm^{-3}, and the total ejected mass is about 15 $M_\odot$. The corresponding velocity field increases almost linearly with distance and can be fitted as

$$v_{ej}(t = t_0) = BR_{ej} , \tag{2.2}$$

where $B = 10^{-5}$ s^{-1}. This distribution is also truncated below 10^{13} cm, and the velocity of the outermost layer of the ejecta is $BR_{ej,0} = 10^4$ km s^{-1}. The resulting total energy of the explosion is about 3×10^{51} ergs, which is somewhat higher than the commonly accepted typical SN energy. This, however, has no consequence in our final results because these distributions are used only to define the fragment stratifications (i.e., we do not follow the effects caused by the whole ejecta but only focus on the fragment evolution): the interfragment medium is defined by equations (2.1) and (2.2), and the fragments have the same distributions but they are a factor ϵ denser.

The initial fragment lengths and locations, which have been rescaled from Figure 1 of Arnett et al. (1989) to the initial ejecta model described above, are given in Table 1. There are two types of fragments defined in the Table, referred to as the *short* and *long* fragments. The initial length is l_0, and R_0 and v_0 are the position and velocity of their leading (fastest) edge, respectively.

The position of a mass element initially located at R_{ej}, evolves during the free-expansion stage as

$$R_{ej}(t) = R_{ej}(1 + Bt) , \tag{2.3}$$

where t is the time elapsed after t_0 (given that t_0 is only 1.85 days, its value is simply set equal to zero in the rest of the discussion). The fragments maintain a homologous growth during the free-expansion stage, and their properties are fully determined once l_0, R_0, ϵ, and the evolutionary time scale are given. The evolution, however, changes when the fragment begins to feel the interaction with the ambient medium via a reverse shock.

2.2. *Fragment Evolution in a Homogeneous Medium*

The interaction of a high-density fragment with the hot gas inside the MSR is followed with the two colliding streams approximation. There are two planar shocks in this approximation: a forward shock, processing the ambient medium, and a reverse shock, penetrating the fragment. They are separated by a shocked region with uniform pressure and, given the fragment growth before interaction, it is assumed that this region can adjust to the continuous changes imposed by fragment expansion. The fragments are considered as cylindrically symmetric and they keep their initial velocity field until shock interaction. The detailed properties of the MSR interior are not known but existing numerical models indicate that the temperatures and densities are roughly uniform (e.g., Tenorio-Tagle et al. 1990b; Igumentshchev et al. 1990). For the sake of simplicity, here we assume that they are uniform within the whole cavity: the temperature is fixed to a single value, $T_a = 10^7$ K, and the densities are considered in the range between $\rho_a \sim 10^{-27}$ to 2×10^{-26} g cm^{-3}. The resulting thermal pressures (within $\sim 10^{-12}$ to 10^{-11} dyn cm^{-2}) are small compared to the fragment *ram* pressure during most of the interaction, and we assume that the fragment destruction rate is solely defined by the ram pressure.

TABLE 1

FRAGMENT PROPERTIES

Type	$l_0/R_{ej,0}$	$R_0/R_{ej,0}$	$v_0/10^3$ km s^{-1}
Short	1/10	1/3	3.3
Long	1/5	1/2	5.0

The two-stream approximation assumes planar shocks with mass conservation on both sides of the colliding flows. The bow shock created by a supersonic fragment, however, is not planar and does not collect the gas mass entering into the shocked region. Instead, the shocked gas streams out of the interaction region and expands into the remnant interior. Thus, here we neglect the inertia of the gas entering into the shocked region, and restrict the analysis to the fragment symmetry axis. The shock front is perpendicular to the radial flow at this point, and the planar shock assumption holds. Also, given the mass loss, the volume that the shocked gas would otherwise occupy is lost and a simple approach to compensate for this loss is to assume that the forward and reverse shocks behave as radiative shocks. This is a sound approximation to derive the dynamical evolution of the reverse shock but is not sufficient to obtain the structure of the shocked region.

With these approximations, it is straightforward to show that the reverse shock will enter into a supersonic fragment at a velocity

$$v_r(t) = \xi v_f(t)\left[\frac{a(t)}{1 + a(t)}\right] , \tag{2.4}$$

with

$$a(t) = \left[\frac{\rho_a}{\rho_r(t)}\right]^{1/2} , \tag{2.5}$$

where $v_f(t)$ is the ejecta velocity just interior to the reverse shock, $\rho_r(t) = A\epsilon R_r(t)^{-3}$ is the fragment density at this same position, $R_r(t)$ is the location of the reverse shock, and ξ is either 4/3 or 1 depending if the shock is adiabatic or isothermal, respectively (as stated above, here we set $\xi = 1$). The reverse shock has an outward speed $v_f(t) - v_r(t)$, and its location is given by

$$R_r(t) = R_0 + \int [v_f(t) - v_r(t)]dt . \tag{2.6}$$

The initial location of the mass element which is being shocked at the time t is $R_{ej} = R_r(t)/(1 + Bt)$. The ejecta velocity is $v_f(t) = BR_{ej} = BR_r(t)/(1 + Bt)$, and the reverse shock velocity can be written as

$$v_r(t) = \frac{B}{1 + Bt} R_r^{5/2}(t)\left[\frac{\chi}{1 + \chi R_r^{3/2}(t)}\right] , \tag{2.7}$$

where $\chi = (\rho_a/A\epsilon)^{1/2}$. Similarly, one can get an analytic expression relating R_r and t

$$\frac{dR_r}{dt} = v_f - v_r = \frac{v_r}{a} = \frac{B}{(1 + Bt)}\left[\frac{R_r}{(1 + \chi R_r^{3/2})}\right] , \tag{2.8}$$

or

$$\ln(R_r/R_0) + \tfrac{2}{3}\chi(R_r^{3/2} - R_0^{3/2}) = \ln(1 + Bt) . \tag{2.9}$$

The right-hand side can also be written as $\ln(R_e/R_0)$, where $R_e = (1 + Bt)R_0$ is where the fragment outer edge would be without the reverse shock. Given that $R_r \gg R_0$, the location of the reverse shock is simply given by the transcendental equation

$$R_r \exp\left(\frac{2\chi R_r^{3/2}}{3}\right) \simeq R_e \,. \tag{2.10}$$

As the fragment is eroded by the reverse shock, the fraction that has been shocked (the processed fraction), f_p, can be written as

$$f_p(t) = \frac{l_p(t)}{l(t)} = \frac{1}{(1 + Bt)l_0}\left\{BR_0 t - \int_0^t [v_f - v_r(t)]dt\right\}, \tag{2.11}$$

where $l(t) = (1 + Bt)l_0 = l_0 R_e/R_0$ is the total length of the fragment in the absence of any interaction, and

$$\begin{aligned} l_p(t) &= R_e - R_r = (1 + Bt)R_0 - R_r(t) \\ &= BR_0 t - \int_0^t [v_f - v_r(t)]dt \,, \end{aligned} \tag{2.12}$$

is the distance traveled by the reverse shock inside the fragment (i.e., the processed length). Thus, the processed fraction can be written as

$$\begin{aligned} f_p(t) &= \frac{(R_e - R_r)}{l_0 R_e/R_0} = \frac{R_0}{l_0}\left(1 - \frac{R_r}{R_e}\right) \\ &\simeq \frac{R_0}{l_0}\left[1 - \exp\left(\frac{-2\chi R_r^{3/2}}{3}\right)\right] \\ &= \frac{R_0}{l_0}\left\{1 - \exp\left[\frac{-2a(t)}{3}\right]\right\}, \end{aligned} \tag{2.13}$$

At early times, the density contrast between the expanding fragment and the ambient medium is very large, and the velocity of the reverse shock remains low. The shock does not penetrate much inside the fragment and affects only a thin layer on its leading side. The erosion process, then, remains as a minor skin effect until the reverse shock accelerates as the density of the expanding fragment drops. Given the set of values for the interior of the MSR and the fragment properties, this occurs at a certain distance, R_E, from the explosion center (i.e., R_E is a reference radius for an effective fragment erosion). Defining this "erosion radius" as the location where $f_p \simeq 5 \times 10^{-2}$ (i.e., where the fragment has been eroded only 5%), which corresponds to $a \simeq 0.03$ or $\rho_r(t) \simeq 1.1 \times 10^3 \rho_a$, one gets

$$R_E \simeq 9.7 \times 10^{-2}\chi^{-2/3} = 6.9\left(\frac{A_{33}\epsilon_{10}}{\rho_{a,27}}\right)^{1/3} \text{pc} \,, \tag{2.14}$$

where $A_{33} = A/10^{33}$, $\epsilon_{10} = \epsilon/10$, and $\rho_{a,27} = \rho_a/10^{-27}$ g. Similarly, the fragment is completely destroyed when $f_p = 1$. This occurs at $a \simeq 0.77$, or $\rho_r(t) \simeq 1.7\rho_a$, and defines the "destruction" radius

$$R_D \simeq 0.84\chi^{-2/3} = 58\left(\frac{A_{33}\epsilon_{10}}{\rho_{a,27}}\right)^{1/3} \text{pc} \,. \tag{2.15}$$

Note that this location is practically *independent of the assumed fragment size*, and provides the limits of influence of any fragmented ejecta. Fragment erosion is complete when the density of the trailing edge has expanded to $1.7\rho_a$.

Figure 1 shows a comparison between a numerical integration of equation (2.11) and the results from a detailed two-dimensional hydrodynamical simulation (see next section). Both calculations refer to the case of the long fragment described in Table 1, with a density contrast $\epsilon = 10$, a homogeneous ambient medium with $T_a = 10^7$ K and $\rho_a = 2 \times 10^{-26}$ g cm^{-3}. The numerical simulations were done with a long fragment expanded to a location of about 1.7×10^{19} cm from the explosion center (i.e., the density of the front part of the fragment was set to $\sim 2 \times 10^{-24}$ g cm^{-3}), but the expanded size was reduced by 12% to partially compensate for the effects of the erosion process. The initial time for this setup corresponds to 1096 yr after explosion. The amount of reduction was set somewhat below the erosion fraction expected from equation (2.13), which is about 16%. The figure shows that, after some initial readjustments of the reverse shock speed in the hydrodynamical simulations, the agreement is better than 5%.

2.3. *X-Ray Emission*

The emission from the shocked gas depends on its chemical abundances, and the compositions of the fragment and MSR interior are different from that of the general interstellar medium. The detailed actual differences, however, are difficult to evaluate. Nonetheless, given the large postshock temperature values (i.e., bremsstrahlung dominates the emission), most of the emission falls in the X-ray region and any variation in the abundances of H and He does not modify the form of the spectrum. For the sake of simplicity, then, here we assume that the relative abundances of the rest of the elements are similar to their cosmic value.

Figure 2 displays the evolution, at three selected times (at

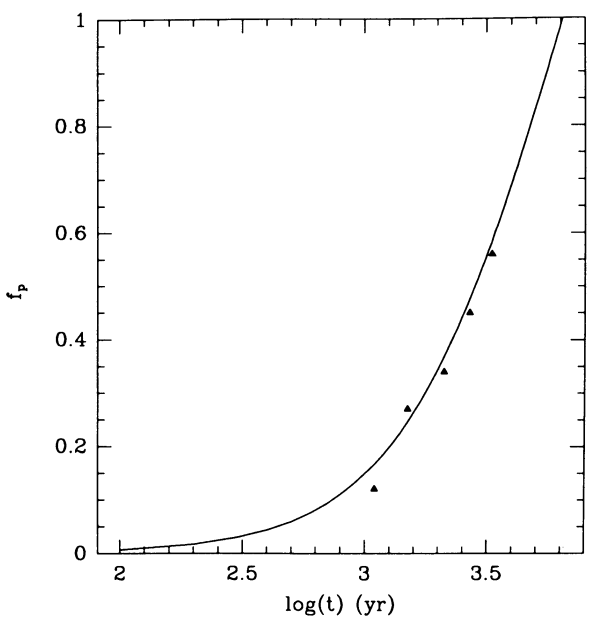

FIG. 1.—Comparison between the analytical solution for fragment erosion (*line*) and the results of two-dimensional numerical simulations along the axis of symmetry (*triangles*) for the long fragment defined in Table 1. The density contrast in the ejecta is $\epsilon = 10$, and the ambient medium has a temperature of $T_a = 10^7$ K and a mass density $\rho_a = 2 \times 10^{-26}$ g cm^{-3}.

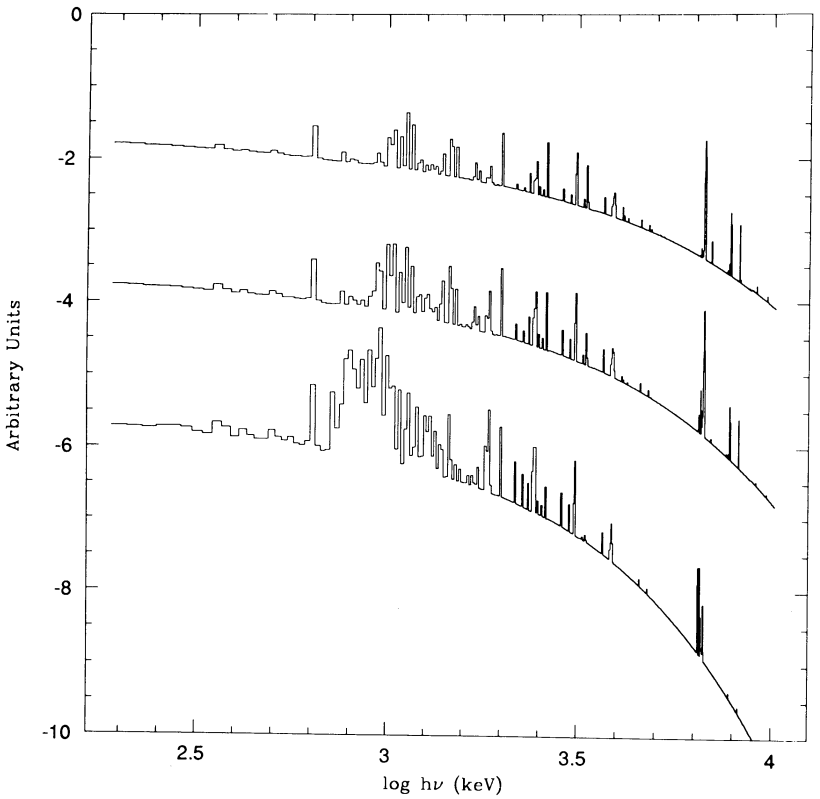

FIG. 2.—X-ray emission per unit volume from a shocked fragment at three selected times. The fragment and ambient parameters correspond to the ones described in Fig. 1. The spectral range is 0.2–10 keV, arranged in bins of 20 eV, and the emission has been arbitrarily normalized to show the details of the three models. The lower spectra corresponds to a time equal to 2×10^3 yr after the SN explosion (close to the third triangle in Fig. 1). The other two correspond to $t = 3 \times 10^3$ yr (*middle*) and $t = 5 \times 10^3$ yr (*upper*).

2×10^3, 3×10^3, and 5×10^3 yr after explosion) of the normalized X-ray spectrum emitted by the shocked fragment presented in Figure 1. The emission, covering the 0.2–10 keV range and arranged in 20 eV bins, was computed with an updated version of the Raymond, Cox, & Smith (1976) code assuming collision equilibrium. The figure shows the equilibrium spectra of gas at the current postshock temperature. The emission at each selected time was normalized, and displaced arbitrarily, to avoid any curve overlapping and to allow for an intercomparison. The continuum becomes harder with time, and line emission decreases, because the reverse shock speeds up as the fragment density decreases.

2.4. *SN Fragments Inside an Expanding MSR*

The final destruction of a fragment occurs either when $f_p = 1$ or when the fragment hits the MSR shell. These two possible cases occur, for any given set of fragment properties, at different MSR evolutionary stages. At early stages, for small MSR radii, the entire fragment or a significant part of it may hit the growing shell. The extreme case occurs when the MSR radius, $R_{\rm MSR}(t)$, is smaller than the erosion radius, R_E, and the colliding fragments are still almost untouched at shell impact. Later on, the shell is reached by smaller and smaller fractions of the original fragments until the MSR radius gets larger than the destruction radius, R_D, and the fragments are fully destroyed within the MSR interior, and do not hit the shell any more.

Assuming a pulsed SN energy injection and an adiabatic evolution, the MSR grows like a wind-driven bubble and one can approximate the external shell radius evolution as (e.g., Mac Low & McCray 1988)

$$R_{\rm MSR}(t) \simeq \left(\frac{125}{154\pi}\right)^{1/5}\left(\frac{L_{\rm SN}\, t_{\rm MSR}^3}{\rho_0}\right)^{1/5} \simeq 78\left(\frac{L_{38}\, t_6^3}{\rho_{0,24}}\right)^{1/5} \text{ pc}\,, \tag{2.16}$$

where $L_{38} = L_{\rm SN}/10^{38}$ ergs s^{-1} is the mechanical luminosity from supernovae exploding every Δt, $\rho_{0,24} = \rho_0/10^{-24}$ g cm^{-3} is the mass density of the external interstellar medium, and $t_6 = t_{\rm MSR}/10^6$ yr is the MSR evolutionary time scale. Using the typical values for all these variables, one can explore the range of parameters in which fragmented ejecta may affect the MSR evolution. In particular, the condition $R_{\rm MSR} = R_D$ provides the maximum time scale for fragment-shell interaction

$$t_{\rm max} \simeq 6.2 \times 10^5\left(\frac{A_{33}\,\epsilon_{10}}{\rho_{a,27}}\right)^{5/9}\left[\frac{\rho_{0,24}}{L_{38}}\right]^{1/3} \text{ yr}\,. \tag{2.17}$$

For $\epsilon_{10} = 10$ (a very dense fragment) and $\rho_{0,24} = 2.3$ (i.e., an ambient volume density of 1 cm^{-3} with 10% helium), $t_{\rm max} \simeq 3 \times 10^6$ yr. Thus, the fragment bombardment phase can last up to a few million years and, for association rates of about one SN per 2×10^5 yr, the first ~ 10 explosions may be able to produce direct fragment-shell collisions.

Figure 3 shows the analytical results for the fragment fraction, $1 - f_p$, hitting the shell as a function of the MSR age $t_{\rm MSR}$. The solution corresponds to an interior density $\rho_{a,27} = 1$. Also, a mechanical luminosity of $L_{38} = 1.6$ was adopted, corresponding to one SN with 10^{51} ergs every $\Delta t = 2 \times 10^5$ yr, and

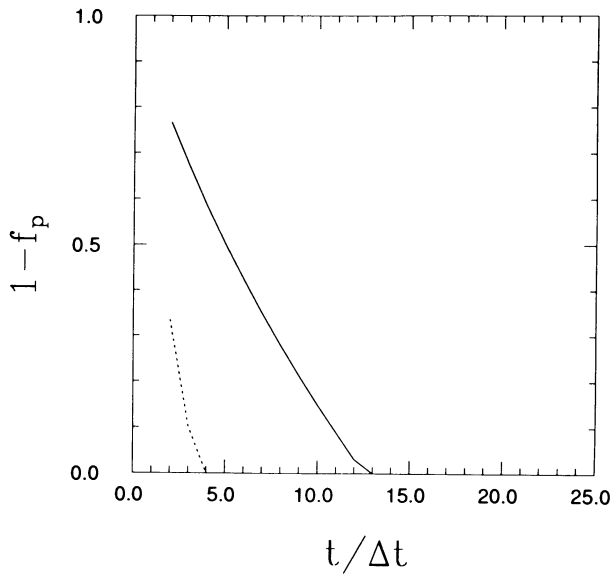

FIG. 3.—Fragment fraction reaching the external shell of a MSR, $1-f_p$, as a function of the MSR evolutionary time in units of $\Delta t = 2 \times 10^5$ yr. The evolution corresponds to the long fragment case, with $T_a = 10^7$ K and $\rho_a = 10^{-27}$ g cm^{-3}. The *solid line* corresponds to a density contrast of $\epsilon = 100$, and the *dashed line* to $\epsilon = 10$.

$\rho_{0,24} = 2.3$. The lines summarize the evolution of fragments originated in each supernova event (starting from the second explosion) for two values of the density contrast, $\epsilon = 100$ (*solid line*) and $\epsilon = 10$ (*dashed line*). As the MSR expands, an increasing fraction of the fragment is shocked within the remnant interior and, finally, after some five to 15 explosions (depending on their density) the fragments are completely thermalized before shell interaction. Given that $R_D \sim \epsilon^{1/3}$, the lower density fragments (*dashed line*) suffer a more substantial erosion and they are completely destroyed after $t_{MSR} \sim 8 \times 10^5$ yr.

Hence, the most important interactions occur at early times and, as in the case of wind-driven bubbles (Tenorio-Tagle et al. 1991; Franco et al. 1991, 1992), the MSRs can be punctured and distorted by fragment collisions. These effects have a profound impact in the further evolution, and, even when the presence of dense blobs is substantially reduced at late times, the early distortions can be present during the rest of the remnant life.

3. NUMERICAL SIMULATIONS

The simulations presented here were done with the two-dimensional hydrodynamical code described by Różyczka (1985). The essential features of this code are the second-order accuracy in spatial coordinates and the axial symmetry imposed on modeled flows. Optically thin radiative cooling (Raymond et al. 1976) was included, but, given the large shock velocities and low postshock densities, it was practically ineffective. The cylindrical grid was composed of 100 × 400 points in the r and z coordinates, respectively, covering a physical area of 10^{19} cm × 4 × 10^{19} cm. The left edge of the grid was located 1.2×10^{19} cm away from the explosion site. On that grid, filled with a uniform medium representing the hot (10^7 K) and tenuous content of the MSR interior, we have followed the evolution of a "long" fragment (see Table 1). The fragment was cut out of the ejecta density and velocity distributions described in § 2, with a density contrast $\epsilon = 10$, and the whole flow was scaled homologously to an outer ejecta radius $R_{ej} = 3.5 \times 10^{19}$ cm. The initial fragment length was set equal to about 6.1×10^{18} cm, corresponding to an eroded fraction of about 12%, and the resulting densities at the top and bottom of the fragment were equal to 2×10^{-24} and 6.75×10^{-24} g cm^{-3}, respectively. The corresponding velocities were bounded between 3.33×10^3 km s^{-1}, at the bottom, and 5×10^3 km s^{-1}, at the top. This initial model corresponds to $t = 3.6 \times 10^{10}$ s after the explosion. The fragment (because of the assumed symmetry, actually only half of it) was placed at the very left of the grid and was allowed to move to the right, along the z-axis. Its angular width was arbitrarily set to 25°, which is about the minimum value providing a reasonable resolution at the beginning of calculations.

Three different runs, corresponding to the same fragment evolving in different ambient conditions, are presented here. In the first case (corresponding to the model discussed in Fig. 1, and now referred to as case A) the density of the MSR interior was set to 2×10^{-26} g cm^{-3}, and in the second one (case B) it was 7 times higher. The assumption of a uniform medium was relaxed in the third run (case C), and a slab of denser gas was placed between the grid locations $z = 2 \times 10^{19}$ cm and $z = 2.6 \times 10^{19}$ cm (i.e., between 3.2×10^{19} cm and 3.8×10^{19} cm from the explosion site), simulating the MSR shell. The slab density was set equal to 1.67×10^{-23} g cm^{-3}, implying a mean density of the surrounding medium of about 6.5×10^{-24} g cm^{-3}, and a total shell mass of about 770 $M_\odot$.

Figure 4 displays the isobaric contours and velocity field of case A at 400, 1.6×10^3, and 2.5×10^3 yr from the beginning of the calculations (i.e., some 1.5×10^3, 2.7×10^3, and 3.6×10^3 yr after the SN explosion). The profile of the relatively unevolved fragment (i.e., the innermost, trapezoidal, grouping of contours) is clearly seen in the first frame, and the velocity spread interior to it is simply due to the initial velocity field of the ejecta. The interaction with the medium produces a leading bow shock (the outermost, pearlike, grouping of contours), whose wings span sideways. Two shocks are immediately driven into the fragment: a very strong reverse shock at the leading edge, and a weaker lateral shock at the side surface. The lateral shock, not taken into account in the analytical considerations, results from the pressure difference between the fragment interior and the gas flowing out of the bow shock (the "back flow"). This shock is unable to penetrate deep into the fragment, as the next two frames show.

The back flow originates at the "horns" seen in Figures 4*b* and 4*c* at the right of the fragment and becomes important as soon as time evolves (the inner boundary of the back flow is visible in Figs. 4*b* and 4*c* as a slightly irregular, almost horizontal, grouping of contours extending beyond the left of the fragment to join the contours outlining the wake). The horns are a cross section of the peripheral parts of the reverse shock, which slows down upon encountering the gas already processed by the lateral shock. The gas squeezed out of the horns acquires a radial velocity component and flows away from the fragment, thus preventing the direct contact between the fragment and the gas of the MSR interior. At later times, the figure also shows that the gas processed by the lateral shock (which is continuously diluted by the overall expansion) expands into the low-pressure region formed between the fragment and the back flow. Due to the screening effect of the horns and the back flow, then, the main body of the fragment remains intact until the arrival of the reverse shock. The same sequence of events occurs in case B (Fig. 5), and the only difference is the strength

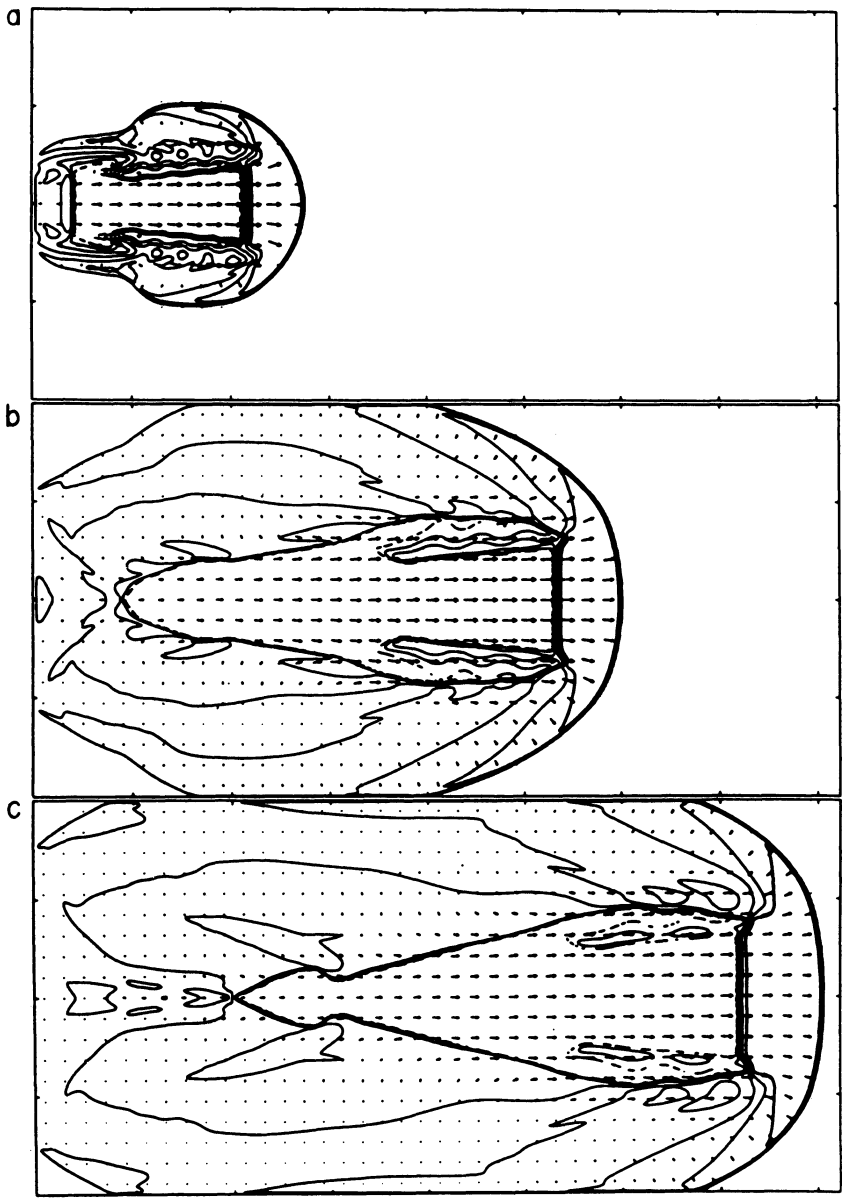

FIG. 4.—Two-dimensional simulation of the evolution of case A (the fragment and ambient parameters are as in Fig. 1). Lines with constant pressure are logarithmically spaced with $\Delta \log p = 0.43$, $\log p_{\min} = -12$ (*broken contour*) and $\log p_{\max} = -9$ (*thickened contour* in the head of the bow shock). The longest arrows in frames (*a*), (*b*), and (*c*) correspond to flow velocities of 4.85, 4.40, and 4.11 $\times$ 10^3 km s^{-1}, respectively. The distance unit between tick marks is 4.85 $\times$ 10^{18} cm. The frames are taken at 400, 1600, and 2500 yr, counting from the beginning of calculations (i.e., some 1500, 2700, and 3600 yr after explosion).

of the shocks driven into the fragment. The lateral shock penetrates deeper in this case, resulting in relatively longer horns. The reverse shock is very fast and overtakes the whole fragment in about 2.7 $\times$ 10^3 yr from the beginning of calculations (at about 3.2 $\times$ 10^3 yr after the explosion).

In case C (Fig. 6), the fragment collides with the MSR shell at $t \sim 1.3 \times 10^3$ yr after the explosion. The reverse shock is strengthened at interaction with the shell, and the fragment is destroyed in about 600 yr. During impact, the gas of the shocked fragment spreads sideways along the inner shell surface, and the transmitted shock propagates (slowly) outward into the shell (Fig. 6*a*). Some 1.9 $\times$ 10^3 yr later, the transmitted shock punctures the shell and begins to sweep through the unperturbed medium surrounding the MSR (Fig. 6b). The collision, then, generates a high-pressure "pocket" at the place of impact, driving a forward shock (termed "secondary blast wave" by McKee 1983) which is able to traverse the shell and promotes the reexpansion of the mixture of shocked fragment and shell gases. This effect is also observed in two dimensional models with higher spatial resolution of a set of fragments colliding with wind-driven shells (Tenorio-Tagle et al. 1991), and some of their results can be applied to MSRs when $f_p < 1$ (i.e., to early evolutionary stages). In particular, neighboring fragment impacts produce an ensemble of small outer shocks which merge into a single "wrapping shock," which moves ahead of the punctured target shell. The gas collected by the wrapping shock eventually collapses into a new cool and dense outer shell, which is surrounding the surviving sections of the original target MSR shell. Such a complicated structure can be viewed as if the punctured shell is also

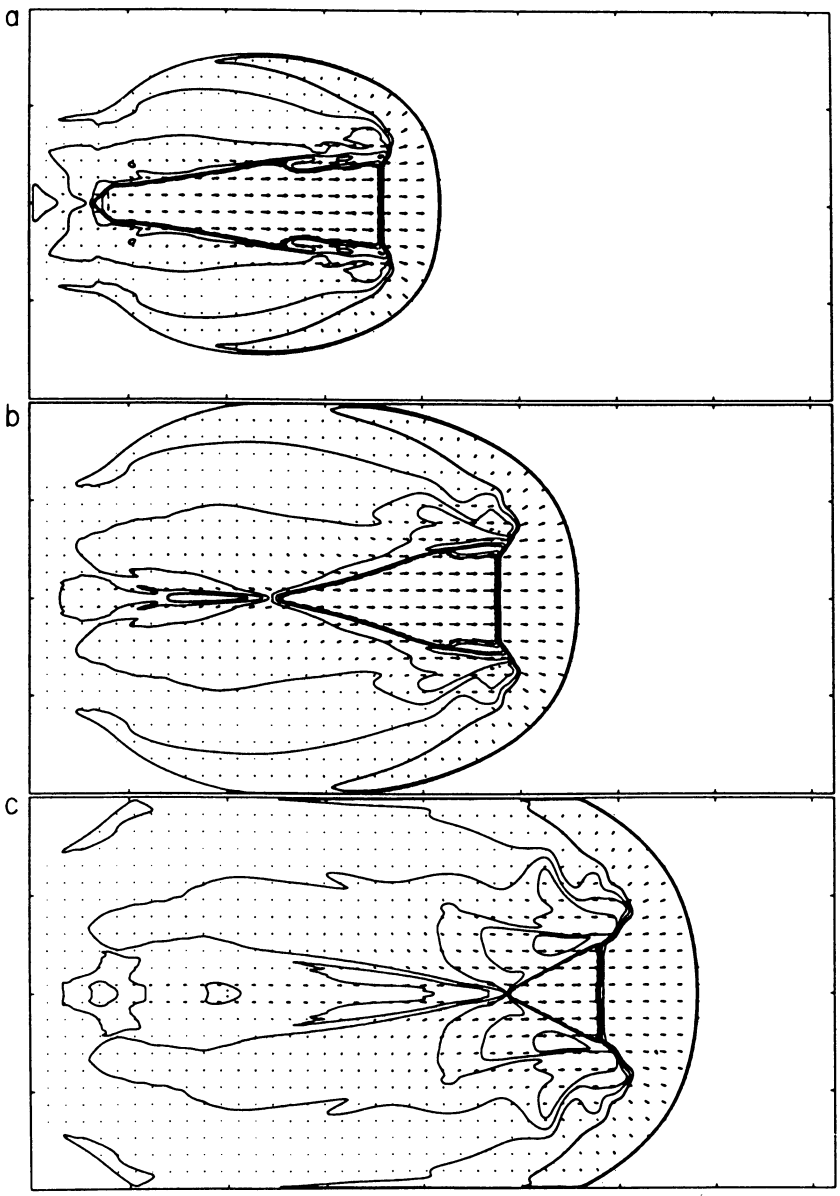

FIG. 5.—The evolution of case B. The distance unit and the contours are the same as in Fig. 4. The longest arrows in each frame correspond to 3.97, 3.66, and 3.29×10^3 km s^{-1}, at 1200, 1900, and 2660 yr, counting from the beginning of calculations (i.e., some 2300, 3000, and 3760 yr after explosion).

capable of forming "clouds." Meanwhile, the disrupted shell material and the shocked supernova fragment gas is efficiently mixed in the interior of the new MSR.

4. DISCUSSION

The matter expelled in SN explosions is not an evenly distributed plasma but rather it seems to contain a collection of fragments with a variety of different sizes, shapes, and density enhancements, ϵ, relative to the interfragment medium. This implies that the details of ejecta thermalization are position-dependent and the resulting energy injection into the ambient medium is anisotropic. Here we have followed the main aspects of this problem and have presented a first step in the analysis of the effects played by the continuous bombardment of SN fragments in expanding MSR. The actual fragment properties are poorly known but, as a first approximation, we have included the range of values inferred from recent explosion simulations. The approach has been focused on the interaction of supersonic fragments with a constant density MSR interior, and the results may be representative of the effects caused by the largest ejected fragments.

The inteaction of the whole ejecta with the MSR interior was not considered but, clearly, the fastest and less dense gas characterizing the outermost parts of the ejecta are rapidly thermalized by a reverse shock. The details of ejecta thermalization, along with the drag experienced by fragments through the thermalized ejecta, will be addressed in a future study. In the case of a dense fragment, the reverse shock begins to be "effective" only after the fragment has reached a distance R_E from the explosion site. Given the MSR interior densities (of the order of 10^{-2} to 10^{-3} cm^{-3}), direct fragment-shell impacts will occur until the fragments are fully thermalized within the

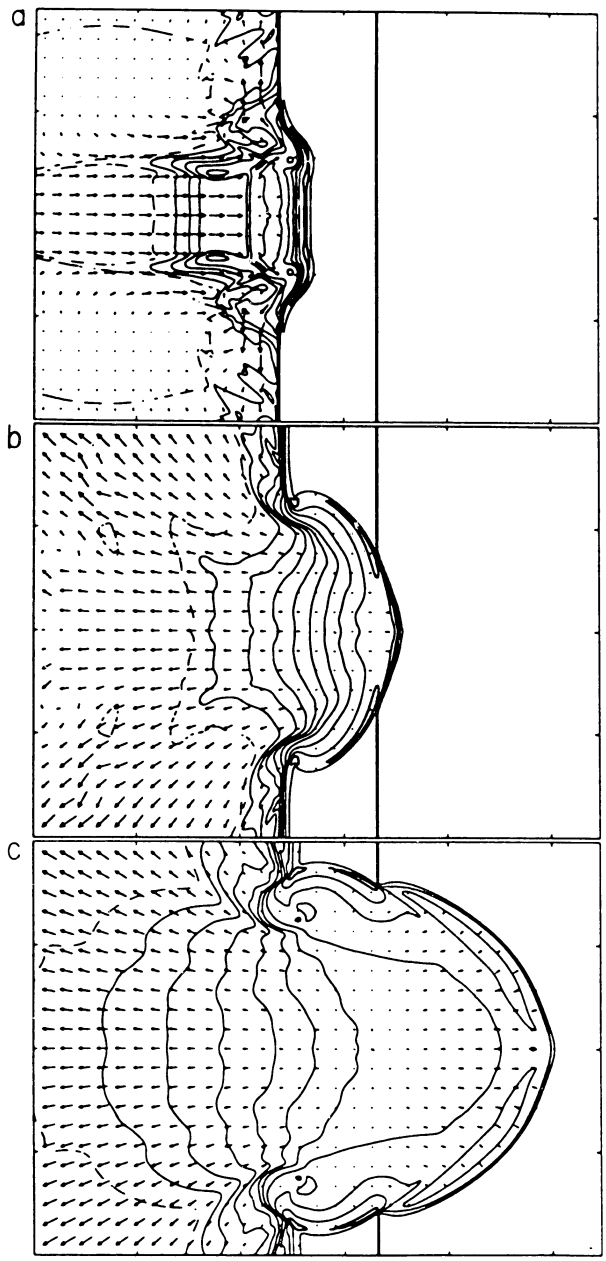

FIG. 6.—The evolution of case C: collision of a fragment with a MSR shell. The distance unit is the same as in Fig. 4. Lines of constant density are logarithmically spaced with $\Delta \log \rho = 0.34$, $\log \rho_{\min} = -25.7$ (*broken*), and $\log \rho_{\max} = -22.3$ (*thickened*). The longest arrows correspond to 4.28, 3.07, and 1.06×10^3 km s^{-1}, at 1600, 3700, and 7700 yr after explosion.

remnant interior (i.e., up to 3×10^6 yr; see Fig. 3). Hence, during the first ~ 15 supernova explosions, an important fraction of the body of those fragments with ϵ in the range 10–100 will impact directly against the expanding MSR shell. This result does not take into account the actual distribution of stars in OB association, which are spread within a radius of several tens of parsecs. Thus, the number of SN explosions leading to a direct impact is in fact underestimated.

One obvious consequence of these direct fragment-shell collisions is that the MSR is excited, reheated, punctured, and distorted after every impact. Figure 6 displays some of the details of shell "perforation" and the "protuberance" generated by the emerging forward shock (see also Figs 5–7 of Tenorio-Tagle et al. 1991, and Fig. 3 of Franco et al. 1991). The size of these protuberances are small compared to the MSR dimensions, but the emerging shocks tend to grow in all directions and, eventually, merge into a single "wrapping" shock. This, in turn, implies that a large fraction of the previously cold shell is in fact reshocked and reheated ($T > 10^6$ K) by fragment collisions, and a new "corrugated" outer shell is formed. Thus, during the first few 10^6 yr, the external "skin" is continuously regenerated, and the remnant growth rate is anisotropic. Shell excitation is also anisotropic and the MSR emission in X-rays (and in many other wavelengths) should be characterized by a series of localized bright spots, indicating the particular places of impact. Also, after shell perforation, the gas flow in the MSR interior becomes turbulent and the mixing of different MSR layers becomes very efficient.

The distortions associated with fragment bombardment operate at small scales, but there exist a variety of additional agents which may induce large-scale deformations. In particular, the density structure of the external medium is a very important factor in defining the overall shape (and growth rate) of the MSR. The negative density gradient along the z-axis (see Dickey & Lockman 1990) defines two important features of the expanding remnant: (1) the polar caps contain less mass per unit surface than the rest of the shell, and (2) the growth rate is faster along the z-axis and, depending on the specific form of the density gradient (e.g., Ostriker & McKee 1988; Franco et al. 1990), the velocity of the main shock front can become ubounded (i.e., the MSR may "blow out" into the halo). Given the lower values of the shell surface mass density, direct impacts in the polar regions generate stronger emerging shocks and these shocks also accelerate with the negative density gradient. Thus, the resulting protuberances are larger along the z-axis.

Although blowout could occur if the density stratifications along the z-axis were described by a single Gaussian distribution, it seems very unlikely in the case of the composite disk atmosphere described by Dickey & Lockman (1990) or when the galactic magnetic field is considered (e.g., Cox 1989; Tomisaka 1992). Nonetheless, if blowout happens to occur the time scales associated with MSR evolution indicate that direct fragment collisions may play a relevant role during these events. A "typical" MSR shell reaches the scale height, H, of a Gaussian distribution (with $H = 100$ pc and a base density of $n_0 = 1$ cm^{-3}) in less than 10^6 yr, and this time increases to about 10^7 yr when evolving through a composite atmosphere with an extended scale height of about 500 pc (see Mac Low & McCray 1988). Hence, for the case of a Gaussian atmosphere, the precursor shocks will blow out earlier than the main shock, and all the reheated matter from previously destroyed shells and the supernova matter could stream into the halo (see De Young & Gallagher 1990).

In summary, the role played by fragmented ejecta in the evolution of MSR is indeed very important. Fragment collisions excite and puncture the MSR shell, and they generate a series of bright spots and protuberances. These are transient features but result in a (long-lasting) corrugated external shell. Also, as a natural response to the density gradient, all these effects tend to be more pronounced along the z-axis. Finally, if blowout occurs, the precursor shocks are accelerated earlier than the main MSR shock and also they become "blowout precursors."

It is a pleasure to thank Harold Yorke for useful comments on an earlier version of the manuscript. Very special thanks to John Raymond, for providing an updated version of his code to compute the radiative cooling of the shocked fragment. A. F., D. P. C., J. F., and M. R. thank the hospitality of the Instituto de Astrofísica de Canarias, Spain, and G. T. T. thanks the hospitality of the Instituto de Astronomía–UNAM, México. The research of D. P. C. was supported by the National Aeronautics and Space Administration under grants NAGW-2532 and NAG 5-629. J. F. and G. T. T. acknowledge the support given to this project by DGAPA-UNAM through the grant IN103991, and EEC grant CI1*-CT91-0935. We also acknowledge the use of the CRAY/YMP of the Supercomputing Center-UNAM, where part of this work was performed. M. R. was supported by the grant KBN 2-1213-91-01 from the Committee for Scientific Research–Poland.

REFERENCES

Alfaro, E. J., Cabrera-Caño, J., & Delgado, A. J. 1991, ApJ, 378, 106
Arnett, D. 1988, ApJ, 331, 377
Arnett, D., Fryxell, B., & Müller, E. 1989, ApJ, 341, L63
Bandiera, R., & van den Bergh, S. 1991, ApJ, 374, 186
Braun, R., Gull, S. F., & Perley, R. 1987, Nature, 327, 395
Brinks, E., & Bajaja, E. 1986, A&A, 169, 14
Bruhweiler, F. C., Gull, T., Kafatos, M., & Sofia, S. 1980, ApJ, 238, L27
Chevalier, R. A., & Klein, R. I. 1978, ApJ, 219, 994
Cowie, L. L., Songaila, A., & York, D. G. 1979, ApJ, 230, 469
Cox, D. P. 1989, in Structure and Dynamics of the ISM, ed. G. Tenorio-Tagle, M. Moles, & J. Melnick (Berlin: Springer Verlag), 500
Cox, D. P., & Smith, B. W. 1974, ApJ, 189, L105
Deul, E., & Hartog, R. H. 1990, A&A, 229, 362
De Young, D. S., & Gallagher, J. S., III. 1990, ApJ, 356, L15
Dickey, J. M., & Lockman, F. J. 1990, ARA&A, 28, 215
Falk, S. W., & Arnett, D. 1973, ApJ, 180, L65
Ferriére, K. M., Mac Low, M. M., & Zweibel, E. 1991, ApJ, 375, 239
Franco, J., Bodenheimer, P., Tenorio-Tagle, G., & Różyczka, M. N. 1992, in Evolution of Interstellar Matter and Dynamics of Galaxies, ed. J. Palouš, W. Burton, & P. O. Linblad (Cambridge: Cambridge Univ. Press), 83
Franco, J., Tenorio-Tagle, G. Bodenheimer, P., & Różyczka, M. N. 1991, PASP, 103, 803
Franco, J., Tenorio-Tagle, G. Bodenheimer, P., Różyczka, M. N., & Mirabel, I. F. 1988, ApJ, 333, 826
Fryxell, B., Arnett, D., & Müller, E. 1991, ApJ, 367, 619
Hachisu, I., Matsuda, T., Nomoto, K., & Shigeyama, T. 1990, ApJ, 358, L57
———. 1991, ApJ, 368, L27
Hamilton, A. J. S. 1985, ApJ, 291, 523
Heiles, C. 1979, ApJ, 229, 533
———. 1984, ApJS, 55, 585
Igumentshchev, I. V., Shustov, B. M., & Tutukov, A. V. 1990, A&A, 234, 396
Kimura, T., & Tosa, M. 1988, MNRAS, 234, 51
Lasker, B. M., & Golinowski, D. A. 1991, ApJ, 371, 563
Lucy, L. B., Danziger, I. J., Gouiffes, C., & Bouchet, P. 1989, in Structure and Dynamics of the ISM, ed. G. Tenorio-Tagle, M. Moles, & J. Melnick (Berlin: Springer-Verlag), 164
Mac Low, M. M., & McCray, R. 1988, ApJ, 324, 776
Mac Low, M. M., McCray, R., & Norman, M. L. 1989, ApJ, 337, 141
McCray, R. 1988, in IAU Colloq. 101, Supernova Remnants and the Interstellar Medium, ed. R. S. Roger & T. L. Landecker (Cambridge: Cambridge Univ. Press), 447
McCray, R., & Kafatos, M. 1987, ApJ, 317, 190
McCray, R., & Snow, T. P., Jr. 1979, ARA&A, 17, 213
McKee, C. F. 1983, in IAU Symp. 101, Supernova Remnants and Theiu X-Ray Emission ed. J. Danziger & P. Gorenstein (Dordrecht: Reidel), 87
McKee, C. F., & Ostriker, J. P. 1977, ApJ, 218, 148
Müller, E., Fryxell, B., & Arnett, D. 1991, in Chemical and Dynamical Evolution of Galaxies, ed. F. Ferrini, J. Franco, & F. Matteucci (Pisa: ETS Editrice), 394
Nomoto, K., Hachisu, I., Matsuda, T., Hashimoto, M., Shigeyama, T., Kumagai, S., & Yamaoka, H. 1991, in Chemical and Dynamical Evolution of Galaxies, ed. F. Ferrini, J. Franco, & F. Matteucci (Pisa: ETS Editrice), 425
Ostriker, J. P., & McKee, C. F. 1988, Rep. Mod. Phys., 60, 1
Palouš, J., Franco, J., & Tenorio-Tagle, G. 1990, A&A, 227, 175
Raymond, J., Cox, D. P., & Smith, B. W. 1976, ApJ, 204, 290
Reynolds, R. J., & Ogden, P. M. 1978, ApJ, 224, 94
———. 1979, ApJ, 229, 942
Różyczka, M. 1985, A&A, 163, 59
———. 1989, in Structure and Dynamics of the ISM, ed. G. Tenorio-Tagle, M. Moles, & J. Melnick (Berlin: Springer Verlag), 463
Salpeter, E. E. 1976, ApJ, 229, 533
Seward, F., Gorenstein, P., & Tucker, W. 1983, ApJ, 266, 287
Tenorio-Tagle, G. 1981, A&A, 94, 338
Tenorio-Tagle, G., & Bodenheimer, P. 1988, ARA&A, 26, 145
Tenorio-Tagle, G., Bodenheimer, P., Franco, J., & Różyczka, M. N. 1990a, MNRAS, 244, 563
Tenorio-Tagle, G., Bodenheimer, P., & Różyczka, M. N. 1987b, A&A, 179, 219
Tenorio-Tagle, G., Różyczka, M., & Bodenheimer, P. 1990b, A&A, 237, 207
Tenorio-Tagle, G., Różyczka, M., Franco, J., & Bodenheimer, P. 1991, MNRAS, in press
Tomisaka, K. 1992, PASJ, 44, in press
Tomisaka, K., Habe, H., & Ikeuchi, S. 1981, Ap&SS, 78, 273
Tomisaka, K., & Ikeuchi, S. 1986, PASJ, 38, 697
van der Hulst, T., & Sancisi, R. 1988, AJ, 95, 1354
Vishniac, E. T. 1983, ApJ, 274, 152
Weaver, R., McCray, R., Castor, J., Shapiro, P., & Moore, R. 1977, ApJ, 218, 377
Winkler, P. F., Tuttle, J. H., Kirshner, R. P., & Irwin, M. J. 1988, in IAU Colloq. 101, Supernova Remants and the Interstellar Medium, ed. R. S. Roger & T. L. Landecker (Cambridge: Cambridge Univ. Press), 65
Woosley, S. E., Pinto, P. A., & Ensman, L. 1988, ApJ, 324, 466